

広島大学学術情報リポジトリ

Hiroshima University Institutional Repository

| | |
|------------|---|
| Title | Cumulative fatigue damage of stress below the fatigue limit in weldment steel under block loading |
| Author(s) | He, Lei; Akebono, Hiroyuki; Sugeta, Atsushi; Hayashi, Yoshiichirou |
| Citation | Fatigue and Fracture of Engineering Materials and Structures , 43 (7) : 1419 - 1432 |
| Issue Date | 2020-06-02 |
| DOI | 10.1111/ffe.13204 |
| Self DOI | |
| URL | https://ir.lib.hiroshima-u.ac.jp/00050511 |
| Right | <p>This is the peer reviewed version of the following article: He, L, Akebono, H, Sugeta, A, Hayashi, Y. Cumulative fatigue damage of stress below the fatigue limit in weldment steel under block loading. Fatigue Fract Eng Mater Struct. 2020; 43: 1419-1432, which has been published in final form at https://doi.org/10.1111/ffe.13204.</p> <p>This article may be used for non-commercial purposes in accordance with Wiley Terms and Conditions for Use of Self-Archived Versions.</p> <p>This is not the published version. Please cite only the published version. この論文は出版社版ではありません。引用の際には出版社版をご確認、ご利用ください。</p> |
| Relation | |



**Cumulative Fatigue Damage of Stress below the Fatigue Limit in Weldment Steel
under Block Loading**

Lei He^a, Hiroyuki Akebono^{a*}, Atsushi Sugeta^a, Yoshiichirou Hayashi^b

^a Department of the Mechanical Science and Engineering, Graduate School of
Engineering, Hiroshima University, 1-4-1 Kagamiyama, Higashi-Hiroshima, Hiroshima
739-8527, Japan

^b Hydropower Dept., Electric Power Development Co.,Ltd, 6-15-1 Ginza, chuo-ku,
Tokyo 104-8165, Japan

*Corresponding author

Tel / Fax : +81-82-424-7538

E-mail address: akebono@hiroshima-u.ac.jp

Abstract

To investigate the cumulative fatigue damage below the fatigue limit of multi-pass weldment martensitic stainless steel, and to clarify the effect of cycle ratios and high stress level in the statement, fatigue tests were conducted under constant and combined high- and low-stress amplitude relative to stress above and below the fatigue limit. The outcomes indicate that neither Modified Miner's nor Haibach approach provided accurate evaluation under repeated two-step amplitude loading. Moreover, effect of cycle ratios has been determined. Additionally, the cumulative fatigue damage saturated model is established and validated. Cumulative fatigue damage contributed by low-stress below the fatigue limit in high stress of 700 MPa is higher than that with 650 MPa at identical conditions (fatigue limit is 575 MPa). Thus, high stress affects fatigue damage behavior below the fatigue limit. A new predicted approach has been proposed based on Corten-Dolan law, whose accuracy and applicability has been proven.

Key words: below fatigue limit, block loading, cumulative fatigue damage, fatigue life prediction, weldment stainless steel

Nomenclature:

D = cumulative fatigue damage value

D_0 = cumulative fatigue damage of one cycle contributed low-stress amplitude below the fatigue limit

D_{Sa} = saturated cumulative fatigue damage contributed low-stress amplitude below the fatigue limit in one block loading

k = slope of $S-N$ curve

m = reciprocal value of the slope of the original $S-N$ curve

n = number of applied cycles

N = number of cycles to failure

n_H = number of cycles of high-stress amplitude applied in one block loading

n_L = number of cycles of low-stress amplitude below the fatigue limit applied in one block loading

N_H = number of cycles to failure at high-stress level

N_f^* = fictitious fatigue life below the fatigue limit

N_L = number of cycles to failure obtained of stress beneath the fatigue limit based on Modified Miner's rule

n_{Sa} = saturation cycles of low-stress amplitude loading below the fatigue limit in one block loading

R = stress ratio

TIG = tungsten inert gas Welding

β = modified coefficient for $S-N$ curve obtained by Corten-Dolan law

θ_l = included angles between a vertical line and the oblique straight portion of $S-N$ curve

σ_H = high-stress amplitude

σ_L = low-stress amplitude below the fatigue limit

σ_w = the fatigue limit

1 INTRODUCTION

As one of the most common rupture modes, fatigue failure frequently arises in engineering components and structures under service loading conditions. It is known that the fatigue behavior of materials dominates fatigue life. In the 1920s, Palmgren¹ creatively introduced the concept of fatigue damage in connection with the number of cycles of applied stress. Since then, many reports have established more exact fatigue damage models for assessing fatigue damage or life under variable amplitude loading²⁻⁷. During the period when damage models were being developed, an interesting phenomenon was found, wherein the so-called conventional fatigue limit under constant amplitude loading vanished when specimens underwent variable amplitude loading; thus, numerous reports have been published in which cumulative fatigue damage laws have been proposed according to the fatigue limit reduction notion⁸, and understanding of the damage process at the microscale level⁹ has been attempted. However, the cumulative fatigue damage laws of fatigue limit reduction models either involve too

many parameters or demand complicated calculation, which limits their application in scientific study and engineering design. Moreover, publications on investigating fatigue damage under variable including cycles below the fatigue limit using kinds of materials have reported^{10,25-26}.

In recent years, hydroelectric power generation has become increasingly popular because it does not harm the environment. As one of the key components, turbine runners serve to convert the gravitational potential energy of water into mechanical energy. A TIG weldment martensitic stainless steel 2RM2 (equivalent to AWS ER410) is used to join turbine runners and crowns by welding. Moreover, this material is also employed to repair cavitation damage formed on the surface of turbine runners after long service periods. Fatigue fracture is one of the main failure modes in hydroelectric turbine runners at the edge of the junction with the crown under service loading conditions that contain high stress (low-frequency: 10^{-8} – 10^{-4} Hz) and low stress (high-frequency: 10–200 Hz)¹¹, even if some of the stress is below the conventional fatigue limit. Thus, understanding the fatigue features of multi-pass weldment martensitic stainless steel under variable amplitude loading, in which low-amplitude loading below the fatigue limit is included, is essential.

With the advancement of industry, fatigue damage behavior below the fatigue limit has received considerable attention from researchers and engineers. Brose¹² conducted fatigue tests under constant stress amplitude below the fatigue limit with periodic overstrain, and initially overstrained followed by stress amplitude below the fatigue limit using three types of steel; the results indicated that specimens could rupture in the above-mentioned test loading pattern except for cases of initially overstrained test followed by stress amplitude smaller than the fatigue limit in SAE 4340 steel. Therefore,

he corrected the $\varepsilon-N$ curve using inelastic strain (removing the elastic portion from total strain), which was recorded by special techniques to replace the total strain and found that the relative fatigue life below the fatigue limit lays on the $\varepsilon-N$ curve of the finite life portion. Thus, he proposed a law by extrapolating the knee point of the original $\varepsilon_{inelastic}-N$ diagram with an identical slope to predict fatigue damage or life under variable amplitude loading. It can be concluded that overstrain affects fatigue damage behavior below the fatigue limit, besides, based on Brose's conclusion, the linear cumulative fatigue damage rule is applicable^{1,14}. However, cycle ratio effect is unknown in this study. Kikukawa¹³ suggested a modified $S-N$ diagram for evaluating fatigue damage in low-carbon steel by measuring the plastic strain range pair induced by stress below the fatigue limit. He also investigated the cycle ratio effect. Because the localization and extremely low value of plastic strain induced by stress below the fatigue limit, which limits the applicability of the approach. In spite of that, the linear accumulated fatigue damage^{1,14} is suggested in the study. Yin¹⁵ investigated fatigue damage under variable amplitude loading, which included strain below the fatigue limit, using case-hardened steels. He established an $\varepsilon-N$ diagram in which the portion below the fatigue limit was determined by employing a linear cumulative fatigue damage law to compute the imaginary fatigue life of the strain amplitude below the fatigue limit by assuming that specimens can fracture under an applied constant strain amplitude. The predicted results using the linear cumulative fatigue damage law showed good agreement with experimental results with respect to periodic overstrain and service loading tests. Additionally, the imaginary fatigue life approach also called fictitious fatigue life seems to be rational. Based on previous reviews, it can be concluded that the classic linear cumulative fatigue damage law^{1,14} is applicable for studying fatigue

damage below the fatigue limit, both under stress and strain control modes. The detailed description of several approaches for evaluating fatigue life including cycles below the fatigue limit based on linear cumulative fatigue damage rule will be introduced in latter.

The mathematical expression of the linear cumulative fatigue damage law is given in Eq.(1), where n and N denote the number of applied cycles and the number of cycles to failure, respectively, at the same constant stress amplitude.

$$D = \sum_{i=1}^m \frac{n_i}{N_i}. \quad (1)$$

Over the past 70 years, numerous articles have been published on cumulative fatigue damage below the fatigue limit under variable and block loading conditions, Fatemi¹⁶ reviewed these approaches. **However**, as was mentioned previously, **these approaches** contain too many parameter or complex calculation process. Additionally, for high cycle fatigue regime, it is difficult to measure plastic strain as mentioned above, thus hysteresis loop energy methods^{4,17-18} seem to lose **their applicability**. Furthermore, linear cumulative fatigue damage rule is widely used in engineering design, considering easy to apply conclusions of the study to engineering application, the linear cumulative fatigue damage rule is determined. It is well known that there are two very famous approaches that are frequently utilized in engineering design to evaluate fatigue damage or life via considering the stress amplitude below the fatigue limit for the $S-N$ curve in bilinear mode. The first one is the Modified Miner's¹⁴ approach, which can be employed to predict fatigue damage below the fatigue limit by extending the $S-N$ curve from the knee point with the same slope of the original $S-N$ curve. And, the second one is Haibach's¹⁹ approach, which provides an assessment procedure by extrapolating the $S-N$ curve from the knee point with a slope factor of $2m-1$, in which m is the reciprocal

value of the slope of the original $S-N$ curve. In addition to these, the Corten-Dolan²⁰ approach can also be utilized to evaluate fatigue damage below the fatigue limit via clockwise rotation of the original $S-N$ curve at a reference point, which is the highest stress amplitude loading in the applied loading pattern. In this method, the modified coefficient β of $\tan\theta_2/\tan\theta_1$, in which θ_1 and θ_2 denote the included angles between a vertical line and the oblique straight portion of the original $S-N$ curve and the rotated line, is suggested to range from 0.7 to 0.95 in that study, which is to the left of the original $S-N$ curve. Similarly, Freudenthal²¹ suggests that a rotating reference point is the stress level corresponding to fatigue life distribution in the 10^3 - to 10^4 -cycle regime, rather than the highest amplitude loading used in a loading pattern. However, for a specific material, the coefficient β cannot be determined without experiment. It has been demonstrated that the Modified Miner's approach can precisely predict fatigue damage under block loading with a force below the fatigue limit for spot welding-joined steel sheets²²⁻²³, whereas Haibach's approach yields accurate evaluation of cumulative fatigue damage in friction stir spot welding-joined steel sheets²⁴. Furthermore, the real damage values of welded steels range from 0.25 to 0.5 when applying Modified Miner's or Haibach's rule has been proposed²⁵⁻²⁶.

The objective of this study is to investigate the cumulative fatigue damage features of weldment martensitic stainless steel 2RM2 for joining and repairing hydroelectric turbine runners under variable amplitude loading below the fatigue limit, as well as to validate the accuracy of the two previously introduced approaches (Modified Miner's and Haibach's rules). A rational evaluative approach is proposed by considering the cycle ratio effect between high- and low-amplitude loading, corresponding to above and below the fatigue limit, and the influence of high stress based on the Corten-Dolan

approach.

2 MATERIAL AND EXPERIMENTAL PROCEDURE

2.1 Material

Round bars were cut from a TIG welding block (base metal AISI CA6NM), whose schematic illustration is shown in Fig.1(a), via electric discharge machining. After that, specimens were manufactured using round bars by lathing, with a minimum diameter of 4.5 mm. The detailed dimensions and shape of the specimen are given in Fig.1(b). The reduced portion of the specimen is weldment 2RM2, which is marked by the shaded area in Fig.1(b). The mechanical properties of utilized material are as follows: 928 MPa of yield strength, 968 MPa of tensile strength, 14.6 % elongation and 7.4 % reduction of area. Its chemical compositions are (mass %): 0.023 C, 0.40 Si, 0.56 Mn, 0.006 P, 0.003 S, 5.14 Ni, 12.63 Cr, 0.31 Mo. The welding conditions are the following: 150-170 A of welding current, 12-14 V of welding voltage, 80-150 mm/min of welding rate, 15 L/min Ar shielding gas, room temperature-150 °C of inter-pass temperature and 135 of number of pass. Prior to fatigue tests, each specimen was polished to a mirror-like surface using sandpaper, ranging from #360 to #2000, and Al₂O₃ powder with a diameter of 1.0 μm. Microstructure of the employed material is displayed in Fig.2 where a representative dendrite can be observed.

2.2 Fatigue test

Fatigue tests were conducted using a hydraulic type MTS 810 high-frequency fatigue test machine with a stress ratio of $R=-1$ under both constant and block loading at room temperature in air. For constant stress amplitude tests, applied frequency was extended from 20 to 60 Hz. For repeated two-step stress amplitude tests, high- and low-stress

amplitudes, corresponding to stress above and below the fatigue limit, were used to investigate the cumulative fatigue damage value contributed by low-stress amplitude. Various cycle ratios were also used to survey the influence of cycle ratio on cumulative fatigue damage below the fatigue limit. The applied frequency of high- and low-stress amplitude was 1 Hz in the high-stress phase, and 50–200 Hz in the low-stress phase for the purpose of decreasing the duration period. Fig.3(a) displays an example of the repeated two-step loading pattern, in which σ_H , σ_L , and σ_w indicate high- and low-stress amplitude and the fatigue limit, respectively; n_H and n_L denote the number of cycles of high- and low-stress amplitude applied in one test block, respectively. First, σ_H and n_H were maintained at constant values of 650 MPa and 10 cycles in one block, respectively, whereas σ_L and n_L were varied in the range from 500 to 300 MPa and from 10^3 and 10^4 cycles in one block. Second, to clarify whether high stress level has an influence on accumulated fatigue damage behavior below the fatigue limit, fatigue tests were also performed under repeated two-step testing conditions, in which σ_H was increased from 650 to 700 MPa, with n_L values of 10^3 and 5×10^3 cycles in one tested block. Low-stress levels were also changed, from 500 to 300 MPa.

Repeated four-step stress amplitude tests, in which only the first step loading amplitude loading was higher than the fatigue limit, were also carried out to validate the accuracy of the proposed fatigue damage evaluative approach for considering damage contributed by stress amplitude loading below the fatigue limit under variable amplitude loading conditions. A schematic illustration of the linear distribution relationship between applied stress and cycles on the semi-log scale and an example of the loading pattern are given in Fig.3(b)(c).

Each fracture surface was observed using an optical microscope (OM) and a scanning

electric microscope (SEM) to identify fatigue cracks originating site.

3 EXPERIMENTAL RESULTS

3.1 Constant stress amplitude

Fatigue test outcomes with surface slip band fracture mode under constant stress amplitude are plotted in Fig.4 on a double logarithmic scale, in which Modified Miner's and Haibach's rules are included. With decreasing stress amplitude, the number of cycles to failure increases rapidly; data unbroken at a stress level relative to 10^7 cycles marked by arrows are defined as the fatigue limit. The $S-N$ curve of test outcomes is included in Fig.4, calculated based on the Society of Materials Science, Japan (JSMS) standard²⁷ and given as Eq.(2). A fatigue limit of 575 MPa was also evaluated on the basis of the JSMS standard. The number of cycles of knee point is 7.486×10^5 . The regression equation for the Modified Miner's rule is the same as Eq.(2), and Haibach's rule is given as Eq.(3)

$$\log_{10}(\sigma) = -0.0685 \log_{10}(N) + 3.1619. (2)$$

$$\log_{10}(\sigma) = -0.0355 \log_{10}(N) + 2.9541. (3) \text{ when } \sigma \leq 575 \text{ MPa}$$

Initiation sites of data points shown in Fig.4 all originated at surface of specimens.

3.2 Repeated two-step stress amplitude

Fatigue test results under repeated two-step stress amplitude loading, in which high-stress amplitude σ_H above the fatigue limit was maintained at constant values of 650 MPa or 700 MPa and low-stress amplitudes below the fatigue limit were varied ranging from 500 to 300 MPa, is listed in Table 1. For both high stress level tested series (with σ_H of 650 and 700 MPa), number of blocks to failure increase with decreasing low stress level below the fatigue limit, additionally, fatigue lives tested under identical σ_H and σ_L are different, thus, the cycle ratio effect can be found. Moreover, for both cycle ratio of $10/10^3$ tested series with different σ_H , number of

blocks to failure are also different under the same stress level, that is to say, the stress levels higher than the fatigue limit affect fatigue lives.

3.3 Fracture Morphology

To identify fatigue cracks originating site, all fracture surfaces were examined using an OM and SEM. A representative fracture surfaces under repeated two-step stress amplitude conditions are shown in Fig.5. It is a typical surface slip band fracture mode. Therefore, the classic linear cumulative fatigue damage rule is applicable.

4 EVALUATION OF RATIONAL APPROACH

4.1 Cumulative fatigue damage based on Modified Miner's rule

Cumulative fatigue damage calculated based on Modified Miner's rule using repeated two-step stress amplitude test results, is shown in Table 2. Number of cycles to failure at 650 MPa and 700 MPa are 1.249×10^5 cycles and 4.233×10^4 cycles, respectively. The cumulative fatigue damage values were calculated using Eq.(1), where n_H and n_L are set experimental parameters, N_H and N_L were acquired from $S-N$ curve, illustration of obtaining N_H and N_L is depicted in Fig.4. The detail values of N_L are list in Table 2. Almost all values are far beneath unity, except three data points in σ_H for 650 MPa with a cycle ratio of $10/10^4$. For results with σ_H of 700 MPa, almost all plots are distributed near 0.1, which indicates that as the high-stress level increases, more damage is contributed by σ_L ; thus, it is understood that the high-stress level affects accumulated fatigue damage beneath the fatigue limit. From the investigation from Joy-A-Ka²⁴, it is well known that the damage sums computed through the Modified Miner's rule is higher than that calculated with Haibach's rule when using the same tested results. In this study, the cumulative fatigue damage value obtained by the Modified Miner's rule

is much lower than unity; thus, the calculated outcomes of cumulative fatigue damage using Haibach's rule are not shown in this study. According to Table 2, one can conclude that the two above-mentioned rules lose their accuracy for evaluating cumulative fatigue damage for the current utilized material under variable amplitude loading conditions, including cycles below the fatigue limit, although they retain accuracy for predicting fatigue damage or life under the above-mentioned condition for friction stir spot welding (FSSW) and spot welded steel sheets²²⁻²⁴, respectively. In summary, neither the Modified Miner's nor Haibach's rule give accurate results.

4.2 Fictitious fatigue life approach

Based on test results in section 3.2, it is clear that the predictive lines beneath the knee point based on Modified Miner's and Haibach's rules give nonconservative estimation of fatigue life for most cases, and several conservative estimations of fatigue life for tested series with high stress of 650 MPa and cycle ratio of 10/10⁴; therefore, a reasonable approach should be proposed. By assuming cumulative fatigue damage equal to unity, fatigue life below the fatigue limit corresponding to a certain stress level can be acquired on the basis of a linear cumulative fatigue damage rule whose expression is given as Eq.(4a)(4b), where N_H and N_f^* indicate the number of cycles to failure at a

$$D = \left(\frac{n_H}{N_H} + \frac{n_L}{N_f^*} \right) \times blocks = 1. \quad (4a)$$

$$N_f^* = \frac{n_L}{\frac{1}{Blocks} - \frac{n_L}{N_H}}. \quad (4b)$$

high-stress level of 650 or 700 MPa in the present study and the fictitious fatigue life below the fatigue limit relative to stress amplitude, respectively. Fictitious fatigue life N_f^* is calculated using Eq.(4b) in which it is assumed that cumulative fatigue damage becoming unity based on repeated two-step amplitude loading test result, in Eq.(4b), n_H ,

n_L are set testing parameters, N_H is constant amplitude loading test result, number of *blocks* to failure are test result under repeated two-step amplitude loading condition, thus fictitious fatigue life can be computed. Because it is a theoretically assumed term for specimens or materials to rupture if subjected to stress amplitude below the fatigue limit with an appropriate number of cycles, according to results calculated using Eq.(4b). However, as a matter of fact, specimens and materials cannot rupture under a constant stress amplitude below the fatigue limit; thus, this term is called fictitious fatigue life. This method has been conducted in the author's previous publications²⁸⁻²⁹, and its applicability has been proven. The computed outcomes are plotted in Fig.6, in which the Modified Miner's rule is also sketched. The data points for constant stress amplitudes were removed, and only the *S-N curve* is plotted. The number of cycles of stress amplitude below the fatigue limit increases with decreasing stress level in both σ_H tested series; this phenomenon is similar to the constant *S-N* feature above the fatigue limit. Furthermore, for σ_H of 650 MPa with cycle ratio of $10/10^4$, three data points whose damage values calculated by the Modified Miner's rule (Table 2) are greater than unity which is the theoretical cumulative fatigue damage value are distributed to the right of the Modified Miner's rule, which indicates that if fictitious fatigue life is to the right of Modified Miner's or Haibach's rule, they will render safe predictions; otherwise, they will afford non-conservative evaluation, which may lead to mechanical accidents in practical industrial applications. Thus, one can see that all data for the $10/10^3$ tested series with both σ_H of 650 and 700 MPa, and $10/5 \times 10^3$ with σ_H of 700 MPa, are distributed to the left of the Modified Miner's rule, and that major data of the $10/10^4$ tested series also distributed to the left of the above-mentioned approach. Therefore, the fictitious fatigue life approach can be applied to interpret the reason Modified Miner's

and Haibach's rules render inaccurate predictions. In both σ_H tested series, the calculated fictitious fatigue lives for $10/10^3$ are shorter than those for $10/5 \times 10^3$ or $10/10^4$ under identical σ_H because of the cycle ratio effect. Additionally, for a cycle ratio of $10/10^3$ in both series, fictitious fatigue lives at identical stress levels with σ_H of 700 MPa are to the left of those of with σ_H of 650 MPa, which shows that specimens and materials will fracture more quickly when subjected to the former σ_H than for a σ_H of 650 MPa with identical σ_L ; in other words, cumulative fatigue damage given by σ_L is linked with applied σ_H .

According to the author's previous reports²⁸⁻²⁹, a critical number of cycles of low-stress amplitude below the fatigue limit exist in one block after being subjected to high-stress amplitude; when exceeding the critical cycles, the stress levels of the former stop damaging specimens or materials, i.e., the remaining cycles become harmless. A microscale damage mechanism for interpretation of the influence of cycle ratios on fatigue damage or fatigue life has been derived in the author's previous publications²⁸⁻²⁹. A brief introduction is elaborated in the present study: after undergoing high-stress amplitude, dislocations are generated and motion on preferentially oriented slip planes dominates to form persistent slip bands (PSBs); when the loading phase transforms from high- to low-stress amplitude below the fatigue limit, the existing dislocations keep moving until reaching grain boundaries, which act as a barrier to impede the motion of dislocations. Because low-stress amplitudes do not have enough force to push dislocations through grain boundaries, dislocations pile up at grain boundaries; thus, the above-mentioned damage saturation region is reached, and after reaching the saturation region, further cycles of low-stress amplitude do not lead to damaging behavior. In the next block, pile up dislocations are released by high-stress amplitude, which leads them

to cross grain boundaries or form new PSBs in adjacent grains. The aforementioned process repeats block to block until specimen rupture.

Fig.7 illustrates the damage process below the fatigue limit with repeated two-step stress amplitude in one block based on the linear cumulative fatigue damage rule, in which the ordinate and abscissa denote cumulative fatigue damage and cycles fraction of low-stress amplitude, fatigue damage accumulates cycle by cycle in a linear relationship, and at certain cycles, it remains constant in one block; this situation is defined as damage saturation. The critical cycles or saturation cycles (n_{sa}) can be calculated on the basis of Eq.(5), where D_0 and D_{sa} indicate the damage in one cycle and the damage at just saturated cycles, respectively.

$$n_{sa} = \frac{D_{sa}}{D_0}. \quad (5)$$

The relationship between cumulative fatigue damage contributed by low-stress amplitude in one block and low-stress amplitude is displayed in Fig.8(a), although scattering exists in the diagram with a σ_H of 650 MPa. The trend of fatigue damage for the $10/10^4$ test series at several stress levels is higher than that of the $10/10^3$ test series; thus the, $10/10^4$ test series is considered to be saturated, and in contrast, the $10/10^3$ series is unsaturated. With a σ_H of 700 MPa, all damage values for the $10/10^3$ tested series are beneath the corresponding stress level for the $10/5 \times 10^3$ tested series; thus, the latter series (diamond marks in Fig.8(a)) has a saturated status, whereas the former data (triangular marks in Fig.8(a)) are treated as unsaturated. Cumulative fatigue damage in one block given by σ_L in σ_H of 700 MPa is almost one order of magnitude higher than those with a σ_H of 650 MPa at identical σ_L . From this, one can conclude that the damage behavior with stress levels below the fatigue limit is remarkably affected by high-stress amplitude. The computed outcomes of saturation cycles with respect to corresponding

stress levels is plotted in Fig.8(b). Because of the scattering of fatigue test results for the 10/10⁴ series with a σ_H of 650 MPa, saturation cycles also exhibit scattering; however, taking into account that the *S-N curve* for the 10/10³ and 10/10⁴ test series show approximately the same slope (Fig.6), it is possible that the saturation cycles remain constant, independent of stress amplitude, below the fatigue limit²⁸⁻²⁹. With a σ_H of 700 MPa, a uniform assumption is also applied. The mean values with σ_H of 650 and 700 MPa are 1433 and 1782 cycles, respectively. These mean values are similar to each other; by considering the data scatter in Fig.8(b), it is deemed that the saturated cycles in one block are also constant, no matter how σ_H is applied. The horizontal line denotes the mean value (1608 cycles for both σ_H of 650 MPa, and for σ_H of 700 MPa) of saturation cycles in Fig.8(b). Additionally, saturation damage in one block is obtained in Fig.8(a) and given as Eq.(6-1) and Eq.(6-2).

$$D_{Sa} = 1.0 \times 10^{-6} e^{0.0153\sigma_L}. (6-1) \quad \text{for } \sigma_H = 650 \text{ MPa}$$

$$D_{Sa} = 6.8 \times 10^{-5} e^{0.0108\sigma_L}. (6-2) \quad \text{for } \sigma_H = 700 \text{ MPa}$$

Furthermore, saturation damage can be expressed as Eq.(7);

$$D_{Sa} = \frac{n_L}{N_f^*}. (7)$$

then, by combining Eq.(6) and Eq.(7), the fictitious fatigue life at arbitrary stress amplitude below the fatigue limit in saturation cycles can be calculated as Eq.(8-1) for a σ_H of 650 MPa when $n_L \geq 1608$

$$N_f^* = \frac{n_L}{1.0 \times 10^{-6} e^{0.0153\sigma_L}}. (8-1) \quad \text{for } \sigma_H = 650 \text{ MPa}$$

cycles, which is the critical number of cycles that low-stress amplitude can contribute to damage effectively. Similarly, when $n_L \geq 1608$ cycles at an applied maximum stress amplitude of 700 MPa, the fictitious fatigue life can be obtained using Eq.(8-2).

$$N_f^* = \frac{n_L}{6.8 \times 10^{-5} e^{0.0108 \sigma_L}} \cdot (8-2) \quad \text{for } \sigma_H = 700 \text{ MPa}$$

The fictitious fatigue lives at respective experimental stress amplitudes calculated utilizing Eq.(8-1) and Eq.(8-2) are shown in Fig.9, where the computed outcomes are consistent with experimental outcomes for both tested series. Therefore, the fictitious fatigue life can be assessed via Eq.(8-1) and Eq.(8-2) if the applied cycle ratio and stress range conforms to the previously deduced saturation statement. Then, by adopting Eq.(1), fatigue damage or fatigue life can be evaluated. For the tested series with a σ_H of 650 MPa, when $n_L < 1608$ cycles, the *S-N curve* of the $10/10^3$ series ought to be utilized to predict fatigue damage or life. Extending the *S-N curve of the $10/10^3$ series*, the intersection point between the original and *modified S-N curve* is at the ordinate of 630 MPa; this value is extremely close to the applied the maximum stress amplitude of 650 MPa in the repeated two-step test. Consequently, it is likely that the Corten-Dolan approach can be applied in the current study. Moreover, for the tested series with a σ_H of 700 MPa, analogously, if $n_L < 1608$ cycles, application of the *S-N curve* of the $10/10^3$ series is essential. It is interesting that after expanding the *S-N curve* of this series, the *S-N curve of $10/10^3$ series* intersects with the *original S-N curve* at a stress level of 720 MPa, which is also similar to the applied maximum (700 MPa). These results suggest that the Corten-Dolan approach leads to accurate evaluation. Fig.10(a) illustrates the Corten-Dolan approach, in which θ_1 and θ_2 are included angles between a vertical line and the oblique straight portion of the original *S-N curve* and the predictive line below the fatigue limit in the unsaturated region. σ_{max} denotes the maximum applied stress level in the loading pattern, and thus a coefficient of β can be computed as Eq.(9).

$$\beta = \frac{\tan \theta_2}{\tan \theta_1} \cdot (9)$$

In fact, $\tan \theta_1$ and $\tan \theta_2$ are the reciprocal of the respective slopes, so Eq.(9) can be rewritten as Eq.(10).

$$\beta = \frac{k_1}{k_2} . (10)$$

where k_1 and k_2 are the slopes of the oblique portion of the original $S-N$ curve and the **modified $S-N$ curve** below the fatigue limit in the unsaturated region, respectively. k_2 is an experimentally determined parameter; thus, k_2 can be obtained by **calculating the $S-N$ curve** of the $10/10^3$ data points from the maximum applied stress level in repeated two-step tests. Comparison of the $S-N$ curve below the fatigue limit for the respective $10/10^3$ tested series and that corrected by the Corten-Dolan approach is shown in Fig.10(b). Obviously, for both tested series, the respective lines between the $S-N$ curve and the Corten-Dolan approach can almost be confused with each other; therefore, the recommendation to utilize the Corten-Dolan approach to predict fatigue damage below the fatigue limit is applicable for the investigated material. In the present study, for a σ_H of 650 MPa, β is 0.38, and for a σ_H of 700 MPa, β is 0.26. From Fig.10(b), it is clear that the two Corten-Dolan lines are almost parallel to each other, so the hypothesis of Corten-Dolan corrected lines with identical slopes at different high-stress levels is possible; in other words, using the mean value of β (0.32) between the two above-mentioned β values is possible. Therefore, the predictive line for various weldment martensitic stainless steels can be acquired by conducting fatigue tests under constant amplitude loading for the purpose of determining k_1 , and then a straight line can be drawn from the ordinate of the applied maximum stress amplitude in the testing loading pattern with a slope of $k_1/0.32$. In conclusion, the Corten-Dolan approach is applicable for predicting cumulative fatigue damage or fatigue life, including loadings below the fatigue limit, for various multi-pass weldment stainless steel materials whose

$S-N$ curves exhibit bilinear characteristics (oblique straight portion-finite life, and horizontal portion-fatigue limit) that resemble the material utilized in the present study.

5 Validation of proposed approach

To verify the accuracy of the proposed approach for predicting cumulative fatigue damage considering cycles below the fatigue limit under variable amplitude loading, confirmation tests were carried out under repeated four-step amplitude loading, whose loading levels and cycles distribution are listed in Table 3. Comparison of predicted and experimental fatigue life results (Table 4) under repeated four-step amplitude loading conditions is plotted in Fig.11. Almost all cases show conservative estimation: experimental results are increased compared with evaluated results, except one case that is slightly smaller than the predicted result. In other words, the aforementioned proposed evaluative approach is suitable for predicting fatigue damage or life, taking into account cycles below the fatigue limit in weldment martensitic stainless steel 2RM2. Cumulative fatigue damage, both including and omitting damage contributed from stress above the fatigue limit, is displayed in Fig.12. Cumulative fatigue damage values decrease slightly after removing damage contributed by cycles above the fatigue limit, which indicates that stress levels below the fatigue limit play an important role in fatigue damage to materials under service-like loading patterns. Considering only cycles above the fatigue limit in engineering design it may lead to mechanical catastrophe; thus, the proposed approach could be utilized to evaluate fatigue damage or life under variable amplitude loading.

6 Summary

To investigate the cumulative fatigue damage behavior of multi-pass weldment martensitic stainless steel, fatigue tests were conducted under combined high- and low-stress amplitude relative to stress level above and below the fatigue limit. The inaccuracy of Modified Miner's and Haibach's rules which supply predictive methods for considering stress amplitude below the fatigue limit, was confirmed. Additionally, the effect of cycle ratios and high stress level on the cumulative fatigue damage below the fatigue limit was clarified. Based on the results, several conclusions can be reached:

- Neither approach provided accurate evaluation under repeated two-step amplitude loading with various cycle ratios, particularly for high-stress of 700 and 650 MPa with $10/10^3$ tested series, because the cumulative fatigue damage values are smaller than these of tested at identical stress level with different cycle ratios. Thus, effect of cycle ratios has been determined. Additionally, the cumulative fatigue damage saturated model is established and validated, in which a critical number of cycles of low amplitude below the fatigue limit in one block exists, when exceeds the value, the remained cycles become harmless.
- For a σ_H of 700 MPa, cumulative fatigue damage contributed by low-amplitude loading below the fatigue limit is higher than that with a σ_H of 650 MPa at an identical cycle ratio and stress level. Thus, the stress level 1.22 times higher than the fatigue limit (575 MPa) has more influence on cumulative fatigue damage behavior below the fatigue limit than that of 1.13 times greater than the fatigue limit.
- A rational evaluative approach has been constructed via the Corten-Dolan procedure on the basis of obtained outcomes under repeated two-step amplitude

loading tests, whose accuracy and applicability were proven via repeated four-step amplitude loading tests.

Acknowledgement

The author is sincerely thanks Electric Power Development Co.,Ltd, Japan for supplying experimental materials and performing TIG welding process. The author is grateful to China Scholarship Council for supporting scholarship in the author's doctoral course.

References

1. Palmgren A. Die Lebensdauer von Kugellagern. *Zeitschrift des Vereines Deutscher Ingenieure*, Berlin, 1924; 68: 339-341.
2. Chaboche J.L. and Lesne P.M. A non-linear Continuous Fatigue Damage Model. *Fatigue Fract Eng Mater Struct*. 1988; 11(1): 1–17.
3. Manson S.S. and Halford. G.R. Practical Implementation of the Double Linear Damage Rule and Damage Curve Approach for Treating Cumulative Fatigue Damage. *Int J Fract*. 1981; 17(2): 169–192.
4. Kujawski D. and Ellyin F. A Cumulative Damage Theory of Fatigue Crack Initiation and Propagation. *Int J Fatig*. 1984; 6(2): 83–88.
5. Pompetzki M.A., Topper T.H. and DuQuesnay D.L. The Effect of Compressive Underloads and Tensile Overloads on Fatigue Accumulation in SAE 1045 steel. *Int J Fatig*. 1990; 12: 207–213.
6. Zhang W and Miller K.J. A Study of Cumulative Fatigue Damage under Variable Loading-mode Condition. *Fatigue Fract Eng Mater Struct*.1996; 19(2):229–239.
7. Kosut J. History Influence Exponent in Cumulative Fatigue Damage Determined Using Two-step Loading Experiments. *Fatigue Fract Eng Mater Struct*.2002; 25:575–586.
8. Bui-Quot T. Cumulative Damage with Interaction Effect Due to Fatigue under Torsion Loading. *Exp Mech*. 1982; 22: 180–187.
9. Miller K.J., Mohamed H.J. and de Ins Rios E.R. Fatigue Damage Accumulation above and below the Fatigue Limit. In Miller K.J. and de Ins Rios E.R eds. *Proceedings of The Behavior of Short Fatigue Cracks*. London, UK: Mechanical Engineering Publications; 1986: 491–511.

10. Sonsino C.M. and Dieterich K. Fatigue design with cast magnesium alloys under constant and variable amplitude loading. *Int J Fatig.* 2006; 28: 183–193.
11. Liu X., Luo Y.Y., and Wang Z.W. A Review on Fatigue Damage Mechanism in Hydro Turbines. *Renewable Sustainable Energy Rev.* 2016; 54: 1–14.
12. Brose W.R., Dowling N.E. and Morrow J. Effect of Periodic Large Strain Cycles on the Fatigue Behavior of Steels. *SAE Trans.* 1974;740221: 1–11.
13. Kikukawa M., Jono M. and Song J. The Cyclic Plastic Strain and Cumulative Fatigue Damage under Actual Loadings (Critical Modified $S-N$ Curve in the Region below the Fatigue Limit). *Trans Jpn Soc Mech Eng.* 1974; 23(252): 743–750. (in Japanese)
14. Miner MA. Cumulative Damage in Fatigue. *J Appl Mech ASME* 1945; 12(3): A159-64.
15. Yin F., Fatemi A. and Bonnen J. Variable Amplitude Fatigue Behavior and Life Predictions of Case-hardened Steels. *Int J Fatig.* 2010; 32: 1126–1135.
16. Fatemi A. and Yang L. Cumulative Fatigue Damage and Life Prediction Theories: a Survey of the State of the Art For Homogeneous Materials. *Int J Fatig.* 1998; 20: 9–34.
17. Golos K. and Ellyin. F. Generalization of Cumulative Damage Criterion to Multilevel Cyclic Loading. *Theor Appl Fract Mec*, 1987; 7: 169–176.
18. Golos1 K. and Ellyin F. A Total Strain Energy Density Theory for Cumulative Fatigue Damage. *J Press Vess-T ASME.* 1998; 110: 36–41.
19. Haibach E. The Allowable Stresses under Variable Amplitude Loading. *Proceedings of the Conference on Fatigue of Welded Structures*, July 6-9, 1970, The Welding Institute, England: 1971: 328–339.
20. Corten H.T. and Dolon T.J. Cumulative Fatigue Damage. *In Proceeding of the International Conference on Fatigue of Metals*. Institution of Mechanical Engineering and American Society of Mechanical Engineers. 1956: 235–246.
21. Freudenthal A.M and Heller R.A. On Stress Interaction in Fatigue and a Cumulative Damage Rule. *J Aerosp Sci.* 1959; 27(7): 431–442.
22. Tanegashima R., Akebono H., Kato M. and Sugeta A. 3-Dimensional Observation of the Interior Fracture Mechanism and Establishment of Cumulative Fatigue Damage Evaluation on Spot Welded Joints Using 590MPa-class Steel. *Int J Fatig.* 2013; 51: 121–131.
23. Tanegashima R., Ohara I., Akebono H., Kato M. and Sugeta A. Cumulative Fatigue Damage Evaluations on Spot-welded Joints Using 590MPa-class Automobile Steel. *Fatigue Fract Eng Mater Struct.* 2015; 38: 870–879.
24. Joy-A-Ka S., Ogawa Y., Akebono H., Kato M., Sugeta A., Sun Y. and Fujii H.

- Fatigue Damage Evaluation of Friction Stir Spot Welded Cross-Tension Joints Under Repeated Two-Step Force Amplitudes. *J Mater Eng Perform.* 2015; 24(6): 2494–2502.
25. Sonsino C.M. Fatigue Testing under Variable Amplitude Loading. *Int J Fatig.* 2007; 29: 1080–1089.
26. Sonsino C.M., Lagoda T. and Demofonti G. Damage Accumulation under Variable Amplitude Loading of Welded Medium- and High-strength Steels. *Int J Fatig.* 2004; 26: 487–495.
27. Sakai T. and Sugeta A. Standard Evaluation Method of Fatigue Reliability for Metallic Materials: Standard Regression Method of $S-N$ Curves. *The Society of Materials Science, Japan.* 2007.
28. He L., Akebono H., Kato M. and Sugeta A. Fatigue Life Prediction Method for AISI 316 Stainless Steel under Variable-amplitude Loading Considering Low-amplitude Loading below the Endurance Limit in the Ultrahigh Cycle Regime. *Int J Fatig.* 2017; 101: 18–26.
29. He L., Akebono H. and Sugeta A. Effect of High-amplitude Loading on Accumulated Fatigue Damage under Variable-amplitude Loading in 316 stainless steel. *Int J Fatig.* 2018; 116: 388–395.

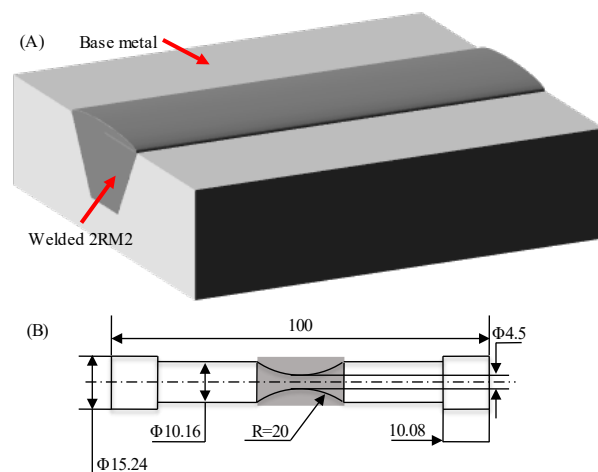


Fig.1(A) Illustration of welding block (B) Shape and dimension of specimen

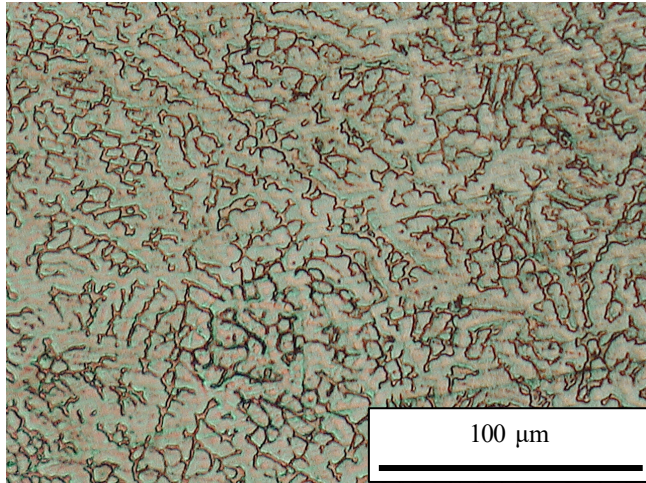


Fig.2 Microstructure of 2RM2

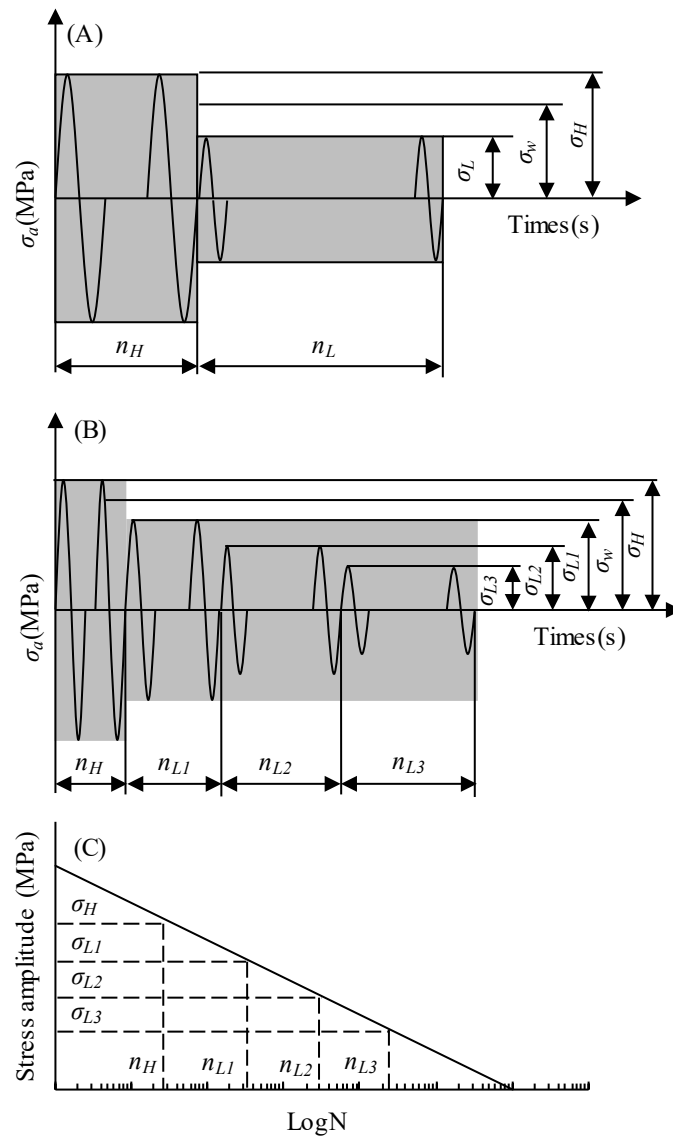


Fig.3(A) Example of repeated two-step amplitude loading pattern (B) repeated four-step amplitude loading (C) Illustration of distribution of applied loading and cycles in repeated four-step test

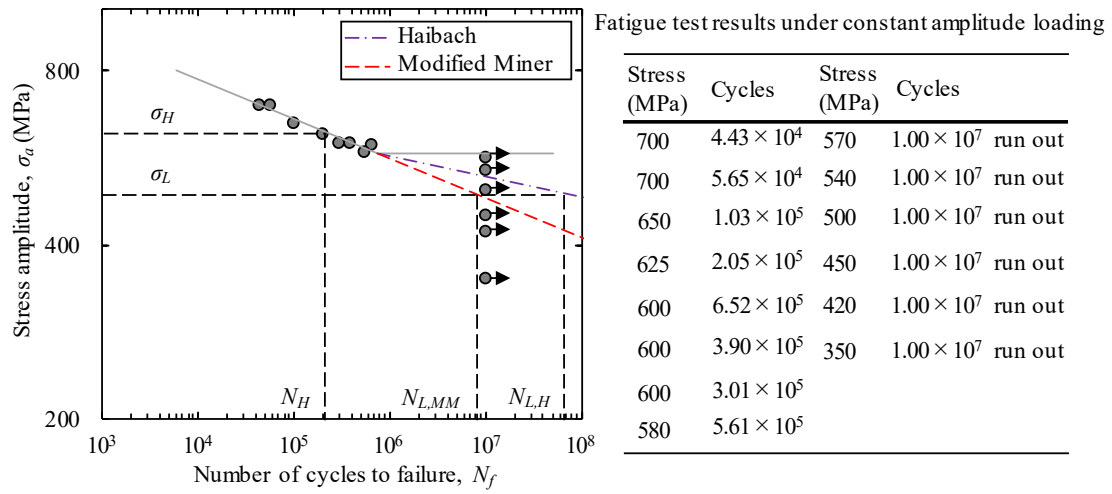


Fig.4 $S-N$ curve of 2RM2 under constant amplitude loading

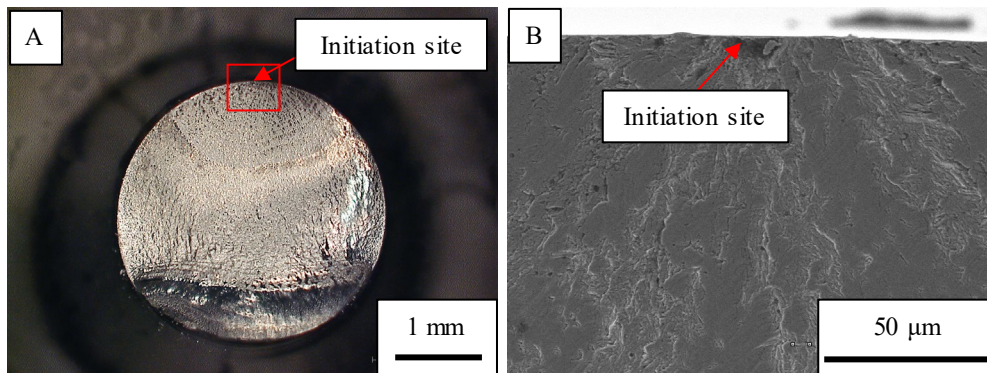


Fig.5 Micrographs of fracture surfaces under repeated two-step amplitude loading with $\sigma_H/\sigma_L = (650 \text{ MPa})/(380 \text{ MPa})$, $n_H/n_L = 10/10^4$, and $N = 5384$ blocks (A) overview of fracture surface; (B) high-magnification image of initiation site

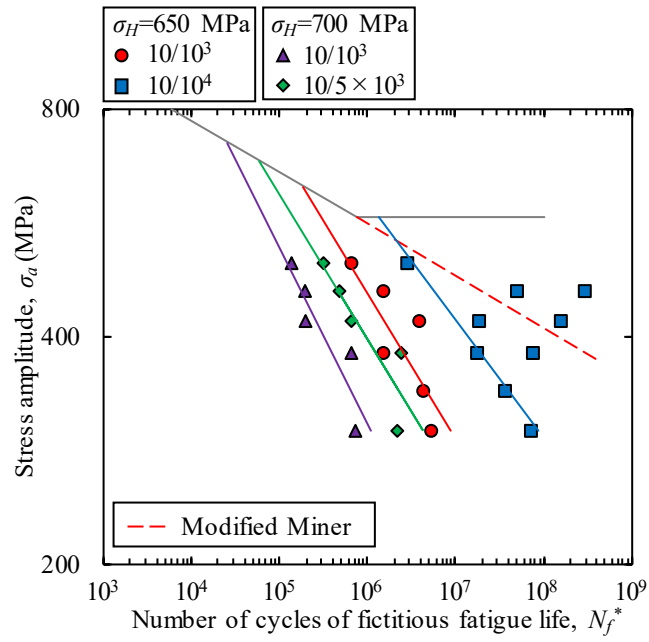


Fig.6 Fictitious fatigue life below the fatigue limit corresponding to respective stress

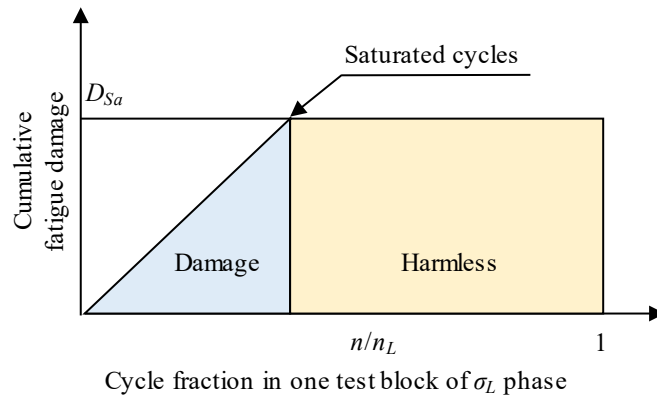


Fig.7 Illustration of damage process when loading is transformed from high to low stress

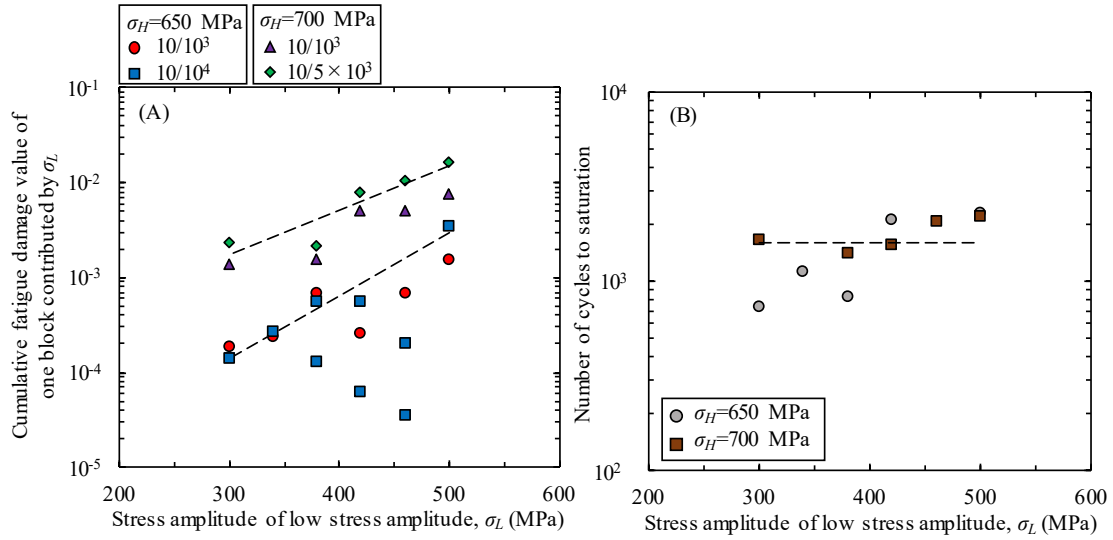


Fig.8(A) Cumulative fatigue damage contributed by low-stress amplitude loading below the fatigue limit against corresponding stress level (B) Saturation cycles of low-amplitude loading below the fatigue limit in one block

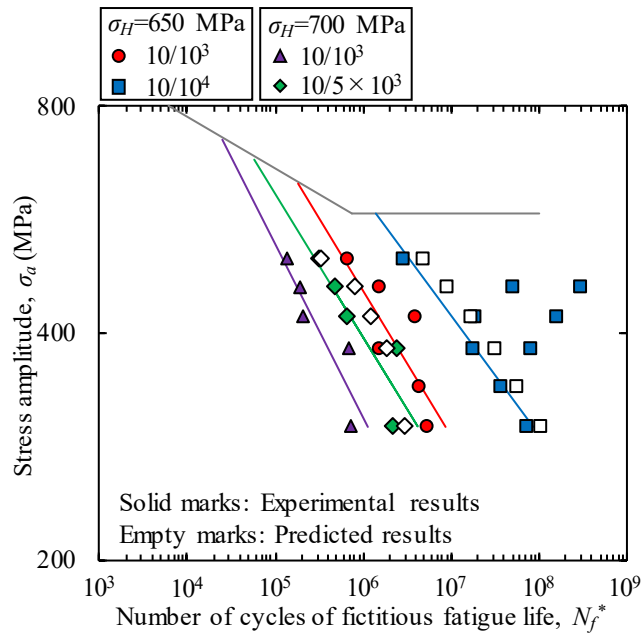


Fig.9 Comparison of fictitious fatigue life between experimental and calculated results

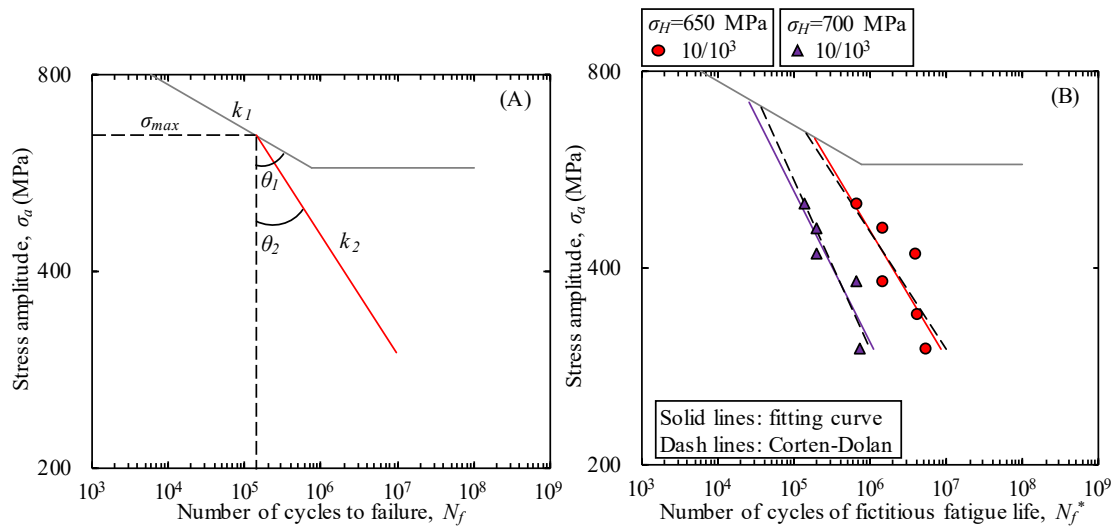


Fig.10 (A) Illustration of the Corten-Dolan approach (B) Comparison of $S-N$ curve of $10/10^3$ series and the Corten-Dolan approach

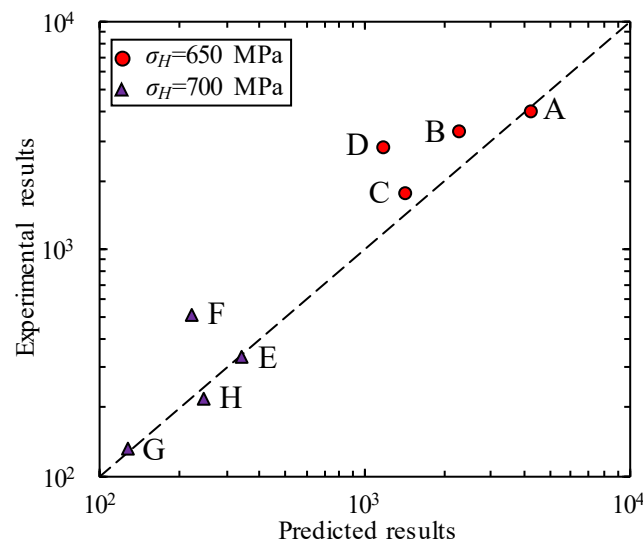


Fig.11 Comparison of experimental and predicted fatigue life under repeated four-step amplitude loading

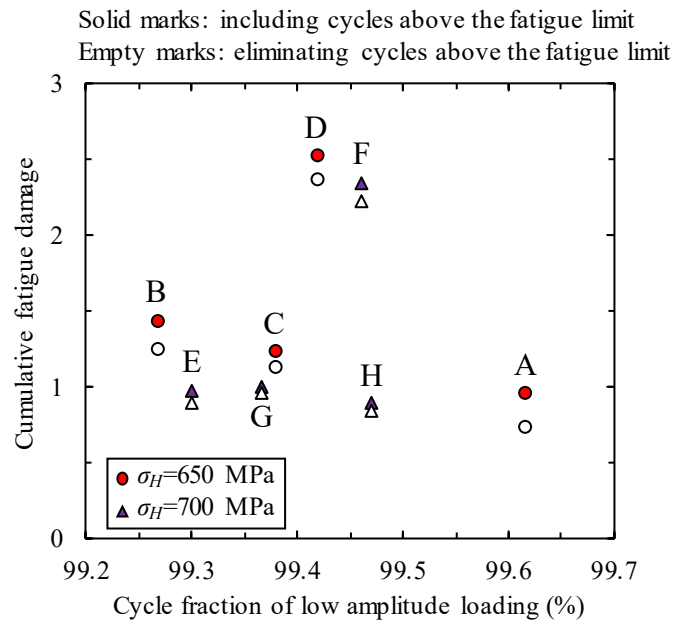


Fig.12 Comparison of cumulative fatigue damage under repeated four-step amplitude loading with stress above the fatigue limit either included or omitted

Table 1 Fatigue test results under repeated two-step amplitude loading

| σ_L (MPa) | Number of blocks to failure | | | |
|------------------|-----------------------------|---------------|--------------------|--------------------|
| | $\sigma_H=650$ MPa | | $\sigma_H=700$ MPa | |
| | $10/10^3$ | $10/10^4$ | $10/10^3$ | $10/5 \times 10^3$ |
| 500 | 630 | 276 | 130 | 60 |
| 460 | 1350 | 10992 3821 | 188 | 93 |
| 420 | 3186 | 8379 1643 | 189 | 123 |
| 380 | 1356 | 1600 5384 | 569 | 419 |
| 340 | 3387 | 1691 | ----- | |
| 300 | 4072 | 5053 | 611 | 389 |

Table 2 Cumulative fatigue damage values based on Modified Miner's rule in repeated two-step amplitude loading tests

| σ_L (MPa) | N_L (Cycles) | $\sigma_H=650$ MPa | | | | $\sigma_H=700$ MPa | | | |
|---------------------|------------------------|------------------------|-------|------------------------|-------|------------------------|-------|------------------------|-------|
| | | $10/10^3$ | | $10/10^4$ | | $10/10^3$ | | $10/5 \times 10^3$ | |
| | | 1 block | Sum |
| 500 | 5.763×10^6 | 2.287×10^{-4} | 0.144 | 1.783×10^{-3} | 0.492 | 4.098×10^{-4} | 0.053 | 1.104×10^{-3} | 0.066 |
| 460 | 1.948×10^7 | 1.071×10^{-4} | 0.145 | 5.671×10^{-4} | 6.234 | 2.876×10^{-4} | 0.054 | 4.930×10^{-4} | 0.046 |
| 420 | 7.354×10^7 | 6.957×10^{-5} | 0.222 | 1.914×10^{-4} | 1.604 | 2.499×10^{-4} | 0.047 | 3.043×10^{-4} | 0.037 |
| 380 | 3.172×10^8 | 5.917×10^{-5} | 0.080 | 8.742×10^{-5} | 0.140 | 2.394×10^{-4} | 0.136 | 2.520×10^{-4} | 0.106 |
| 340 | 1.610×10^9 | 5.665×10^{-5} | 0.192 | 6.222×10^{-5} | 0.188 | ----- | | | |
| 300 | 1.001×10^{10} | 5.614×10^{-5} | 0.229 | 5.703×10^{-5} | 0.288 | 2.364×10^{-4} | 0.144 | 2.368×10^{-4} | 0.092 |

Note: For $\sigma_H=650$ MPa test series, please take n_H as 7 cycles (set value 10 cycles), and n_L as 995 (set value 10^3 cycles) or 9954 cycles (set value 10^4 cycles); for $\sigma_H=700$ MPa test series, re-calculation using the cycle ratios given in Table 2 is reproducible.

Table 3 Test conditions of repeated four-step tests

| | Waveform A | Waveform B | Waveform C | Waveform D |
|---------------------|------------|------------|------------|------------|
| σ_H (MPa) | 650* | 650* | 650* | 650* |
| σ_{L1} (MPa) | 450 | 520 | 480 | 470 |
| σ_{L2} (MPa) | 320 | 400 | 400 | 410 |
| σ_{L3} (MPa) | 200 | 310 | 350 | 370 |
| n_H (Cycles) | 10 | | | |
| n_{L1} (Cycles) | 105 | 58 | 136 | 193 |
| n_{L2} (Cycles) | 487 | 296 | 464 | 518 |
| n_{L3} (Cycles) | 2000 | 1000 | 1000 | 1000 |
| | Waveform E | Waveform F | Waveform G | Waveform H |
| σ_H (MPa) | 700* | 700* | 700* | 700* |
| σ_{L1} (MPa) | 500 | 450 | 520 | 510 |
| σ_{L2} (MPa) | 400 | 380 | 480 | 380 |
| σ_{L3} (MPa) | 300 | 340 | 420 | 320 |
| n_H (Cycles) | 10 | | | |
| n_{L1} (Cycles) | 100 | 245 | 193 | 110 |
| n_{L2} (Cycles) | 316 | 600 | 373 | 563 |
| n_{L3} (Cycles) | 1000 | 1000 | 1000 | 1200 |

*Stress level above the fatigue limit

Table 4 Fatigue test results under repeated four-step amplitude loading

| | Waveform A | Waveform B | Waveform C | Waveform D |
|-------------------|------------|------------|------------|------------|
| Blocks to failure | 4051 | 3271 | 1756 | 2802 |
| | Waveform E | Waveform F | Waveform G | Waveform H |
| Blocks to failure | 334 | 513 | 132 | 221 |